SCIENTIFIC REPORTS

OPEN

Anomalous isotope effect in iron-based superconductors

Wen-Min Huang[1] & Hsiu-Hau Lin [ID] [2]

The role of electron-phonon interactions in iron-based superconductor is currently under debate with conflicting experimental reports on the isotope effect. To address this important issue, we employ the renormalization-group method to investigate the competition between electron-electron and electron-phonon interactions in these materials. The renormalization-group analysis shows that the ground state is a phonon-dressed unconventional superconductor: the dominant electronic interactions account for pairing mechanism while electron-phonon interactions are subdominant. Because of the phonon dressing, the isotope effect of the critical temperature can be normal or reversed, depending on whether the retarded intra- or inter-band interactions are altered upon isotope substitutions. The connection between the anomalous isotope effect and the unconventional pairing symmetry is discussed at the end.

Superconductivity[1–5] is a novel phenomenon of zero electric resistance in some materials when cooled below the characteristic critical temperature T_c. The magic arises from electron pairing in superconductors such that the low-energy excitations are described by an exotic quantum condensate without any dissipation. In conventional superconductors, such as aluminium, the interactions between electrons and the lattice vibrations generate effective attraction and lead to electron pair formation. In quantum language, these vibrations can be treated as particle-like excitations named phonons. It is generally believed that the electron-phonon interactions explain the pairing mechanism for conventional superconductors.

On the contrary, the pairing mechanism of the unconventional superconductors, such as cuprates, seems to stem from the strong electron-electron interactions. Despite of intensive experimental and theoretical studies[1,2] in the past decades, there are still plenty of unsettled controversies about these unconventional superconductors. One of the most important issues is the interplay between the electron-electron and the electron-phonon interactions[6–18]. The recently discovered iron-based superconductors[3–5,19–23] provide a unique testing ground to address this issue[24–27]. Gathered from theoretical and experimental investigations, the interaction strength in the iron-based superconductors is only weak to medium, rendering controlled theoretical understanding possible.

One of the checking points is the critical temperature of superconductivity upon isotope substitutions[28–31]. According to the Bardeen-Cooper-Schrieffer theory for the conventional superconductors, the critical temperature T_c is related to the mass of the isotope element M,

$$T_c \sim M^{-\alpha}, \qquad (1)$$

where α is the exponent for the isotope effect. If the dominant interaction is electron-phonon in nature, theoretical calculations give $\alpha = 1/2$. In the extreme opposite, if the pairing is completely driven by electron-electron interactions, the critical temperature should not change with isotope substitutions and the corresponding exponent is $\alpha \approx 0$. In realistic superconductors, we expect the isotope exponent to be in-between. Note that, in unconventional superconductors, the phonon-mediated interactions are insufficient to explain the pairing mechanism and it is of crucial importance to study the interplay between electron-electron and electron-phonon interactions[24–27]. For instance, even when the pairing mechanism is electronic origin, dispersions observed in angle-resolved photoemission spectroscopy manifest distortions upon isotope substitutions[13–18,27].

The isotope effect observed in iron-based superconductor[28–34] seems to tell a more complicated story. For instance, a strong isotope effect by iron substitution[28] is found in SmFeAs(O, F) and (Ba, K)Fe$_2$As$_2$, almost as large as that in conventional superconductors. On the contrary, *inverse* isotope effect[29] is spotted in (Ba, K)Fe$_2$As$_2$ with different isotope substitutions. Later, it was proposed that the isotope substitutions may give rise to structural change[35] and further complicate the story. On the theoretical side, Yanagisawa *et al.*[36] proposed a

¹Department of Physics, National Chung Hsing University, 40227, Taichung, Taiwan. ²Department of Physics, National Tsing Hua University, 30013, Hsinchu, Taiwan. Correspondence and requests for materials should be addressed to W.-M.H. (email: wenmin@phys.nchu.edu.tw) or H.-H.L. (email: hsiuhau.lin@gmail.com)
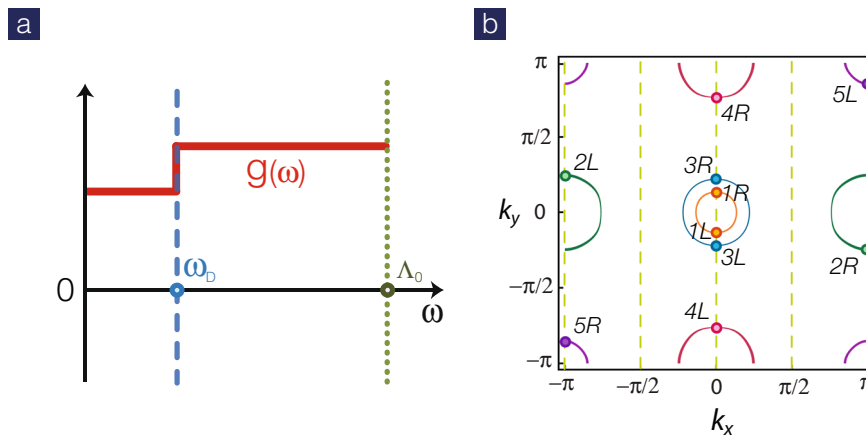
1

Figure 1. (**a**) Step-like interaction profile for simultaneous and retarded interactions. A sharp step is assumed at the Debye frequency ω_D. (**b**) Fermiology of the five-band model $x = 0.1$. These Fermi surfaces are well sampled by five pairs of Fermi points, equivalent to the four-leg geometry with quantized momenta (dashed lines).

multi-band and multi-channel model to explain the possibility of observing the inverse isotope effect. However, Bussmann-Holder and Keller[37] commented that an inversion of the exponent cannot occur upon iron isotope substitutions. The controversies about the isotope effect of the iron-based superconductor are still on. And, it is of crucial importance to clarify the subtle role of the electron-phonon interactions in iron-based superconductors.

Results

Instantaneous and retarded interactions.   Motivated by the controversy, we investigate the competition between electron-electron and electron-phonon interactions by the unbiased renormalization-group (RG) method. Due to the retarded nature of the phonon-mediated interactions, the energy dependence must be included. The minimal approach to include both simultaneous and retarded interactions can be accomplished by the step-shape approximation[38–41] as shown in Fig. 1(a),

$$g_i(\omega) = g_i + \widetilde{g}_i \Theta(\omega_D - \omega), \tag{2}$$

where g_i and $\widetilde{g}_i$ represent (instantaneous) electronic interactions and (retarded) phonon-mediated ones. The energy scale for the retarded interactions is set by the Debye frequency ω_D. Our RG analysis reveals that the pairing mechanism is dominated by the electronic interactions g_i. But, the retarded interactions $\widetilde{g}_i$ also grow under RG transformation and become relevant in low-energy limit. Inclusion of these subdominant interactions leads to anomalous isotope effect. The isotope exponent α can be extracted numerically from RG flows in weak coupling. It is quite remarkable that the sign of the exponent α sensitively depends on whether the inter- and/or intra-band interactions are altered by isotope substitutions.

Multi-band model.   To illustrate how the RG scheme works, we start with a five-orbital tight-binding model for iron-based superconductors with generalized on-site interactions,

$$
\begin{aligned}
H = {} & \sum_{\boldsymbol{p},a,b} \sum_{\alpha} c_{\boldsymbol{p}a\alpha}^{\dagger} K_{ab}(\boldsymbol{p}) c_{\boldsymbol{p}b\alpha} + U_1 \sum_{i,a} n_{ia\uparrow} n_{ia\downarrow} \\
& + U_2 \sum_{i,a<b} \sum_{\alpha,\beta} n_{ia\alpha} n_{ib\beta} + J_H \sum_{i,a<b} \sum_{\alpha,\beta} c_{ia\alpha}^{\dagger} c_{ib\alpha} c_{ib\beta}^{\dagger} c_{ia\beta} \\
& + J_H \sum_{i,a<b} [c_{ia\uparrow}^{\dagger} c_{ia\downarrow}^{\dagger} c_{ib\downarrow} c_{ib\uparrow} + \text{H.c.}]\},
\end{aligned}
\tag{3}
$$

where a, $b = 1, 2, \ldots, 5$ label the five d-orbitals of Fe, 1: $d_{3Z^2-R^2}$, 2: d_{XZ}, 3: d_{YZ}, 4: $d_{X^2-Y^2}$, 5: d_{XY}, and $\alpha = \uparrow, \downarrow$ is the spin index. The kinetic matrix K_{ab} in the momentum space has been constructed in previous studies[42]. The generalized on-site interactions consist of three parts: intra-orbital U_1, inter-orbital U_2 and Hund's coupling J_H. Adopted from previous studies, we choose the values, $U_1 = 4$ eV, $U_2 = 2$ eV and $J_H = 0.7$ eV for numerical studies here.

Fermiology is important in the multi-band superconductors. The electron doping x is related to the band filling $n = 6 + x$ ($n = 10$ for completely filled bands) here and the Fermi surface at $x = 0.1$ is illustrated in Fig. 1(b). There are five active bands: two hole pockets centered at $(0, 0)$ and another hole pocket centered at (π, π) while two electron pockets located at $(\pi, 0)$ and $(0, \pi)$ points[43]. To simplify the RG analysis, we sample each pocket with one pair of Fermi points (required by time-reversal symmetry). This is equivalent to a four-leg ladder geometry with quantized momenta as shown in Fig. 1(b). In the low-energy limit, the effective Hamiltonian[44–46] is captured by five pairs of chiral fermions with different velocities. The RG equations for all couplings can be found in Methods.
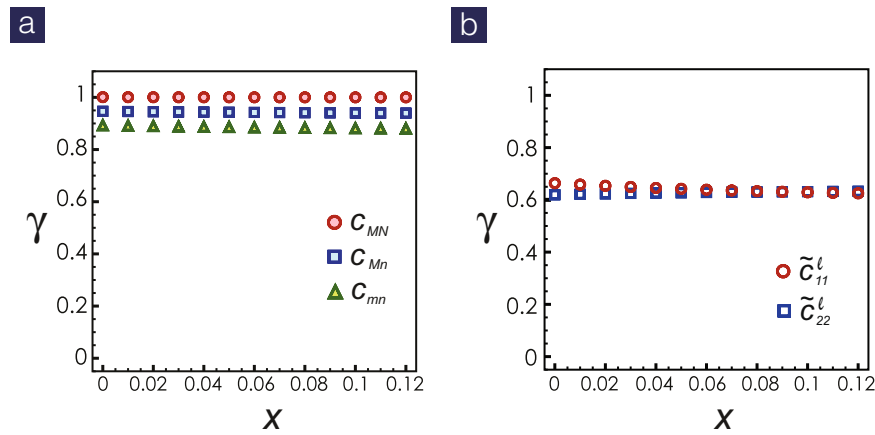
Figure 2. RG exponents for (**a**) the simultaneous and (**b**) the retarded Cooper scatterings. The dominant interactions are pairing hopping between and within band 1 and band 2, with maximal exponent of unity, while other relevant couplings are subdominant with RG exponent smaller than one.

Pairing mechanism. By integrating the two sets of RG equations numerically, we found all couplings are well described the scaling ansatz[47],

$$g_i \approx \frac{G_i}{(l_d - l)^{\gamma_{g_i}}}, \; \widetilde{g}_i \approx \frac{\widetilde{G}_i}{(l_d - l)^{\gamma_{\widetilde{g}_i}}}, \tag{4}$$

where $G_i, \widetilde{G}_i$ are non-universal constants and $\gamma_{g_i}, \gamma_{\widetilde{g}_i}$ are RG exponents for simultaneous and retarded couplings. The divergent length scale l_d, associated with the pairing gap, is solely determined by electronic origin. The dominant pairing occur within band 1 and band 2 and the Cooper scatterings c_{11}, c_{22} c_{12} have maximum exponent $\gamma_i = 1$. Other Cooper scatterings are subdominant with exponents close to 0.9, as shown in Fig. 2(a). Meanwhile, by Abelian bosonization[45,46], the signs of c_{ij} from numerics lead to sign-revised (between electron and hole pockets) $s_\pm$-wave pairing, agreeing with the previous functional RG study[48]. Note that these exponents are rather robust within the doping range where the same Fermiology maintains. What about the phonon-mediated interactions? As clearly indicated in Fig. 2(b), the RG exponents for $\widetilde{c}_{11}, \widetilde{c}_{22}$ are roughly 0.6, much smaller than the dominant electronic interactions, showing the pairing mechanism is electronic origin. However, since the RG exponents are positive, the retarded interactions also grow under RG transformation. These subdominant phonon-mediated interactions can lead to anomalous isotope effect as explained in the following.

Two-step RG scheme. To achieve quantitative understanding in weak coupling, the rescaled Debye frequency must be taken into account carefully. Under RG transformations, $\omega_D \to \omega_D e^l$ as shown in Fig. 3. At the (logarithmic) length scale $l_D \equiv \log(\Lambda_0/\omega_D)$, the difference between g_i and $\widetilde{g}_i$ disappears. The Debye frequency $\omega_D \sim 30\,\text{meV}$ in iron-based materials[24] and the band width (thus Λ_0) is 3–4 eV, giving rise to $l_D \sim 5$. Note that the RG is truncated at the cutoff length scale l_c where the maximal coupling reaches order one. In weak coupling, it is clear that $l_c > l_D$ and thus the RG scheme must be divided into two steps. For $l < l_D$, both sets of RG equations are employed. At $l = l_D$, the functional form for the retarded interactions is the same as the instantaneous one. Thus, one should add up both types of couplings $g_i(l_D) + \widetilde{g}_i(l_D)$ and keep running RG by just the first set of equations. In physics terms, this means that the difference between simultaneous and retarded interactions vanishes before the pairing gaps open.

Extracting isotope exponent. Numerical results for the two-step RG indicate the same superconducting phase as described in previous paragraphs but the isotope exponent α can be extracted numerically. Under RG transformation, the critical temperature satisfies the scaling form, $k_B T_c \sim \Delta[g(0)] = \Delta_c e^{-l_c}$, where Δ_c is the pairing gap at the cutoff length scale. By varying the length scale l_D, the critical temperature changes, i.e.

$$\frac{d(\log T_c)}{dl_D} \approx \frac{d(\log \Delta_c)}{dl_D} - \frac{dl_c}{dl_D}. \tag{5}$$

Furthermore, from the definition of the isotope exponent, the standard scaling argument under RG transformation gives rise to the isotope exponent.

$$\alpha \equiv -\frac{d(\log T_c)}{d(\log M)} \approx \frac{1}{2}\frac{d(\log \Delta_c)}{d(\log \omega_D)} + \frac{1}{2}\frac{dl_c}{dl_D}, \tag{6}$$

where $d(\log M) = -2d(\log \omega_D) = 2dl_D$, because $\omega_D \sim M^{-1/2}$. The above formula for the isotope exponent α is the central result in this paper. For conventional superconductor, $\Delta_c \sim \omega_D$ and the cutoff length scale is not sen-
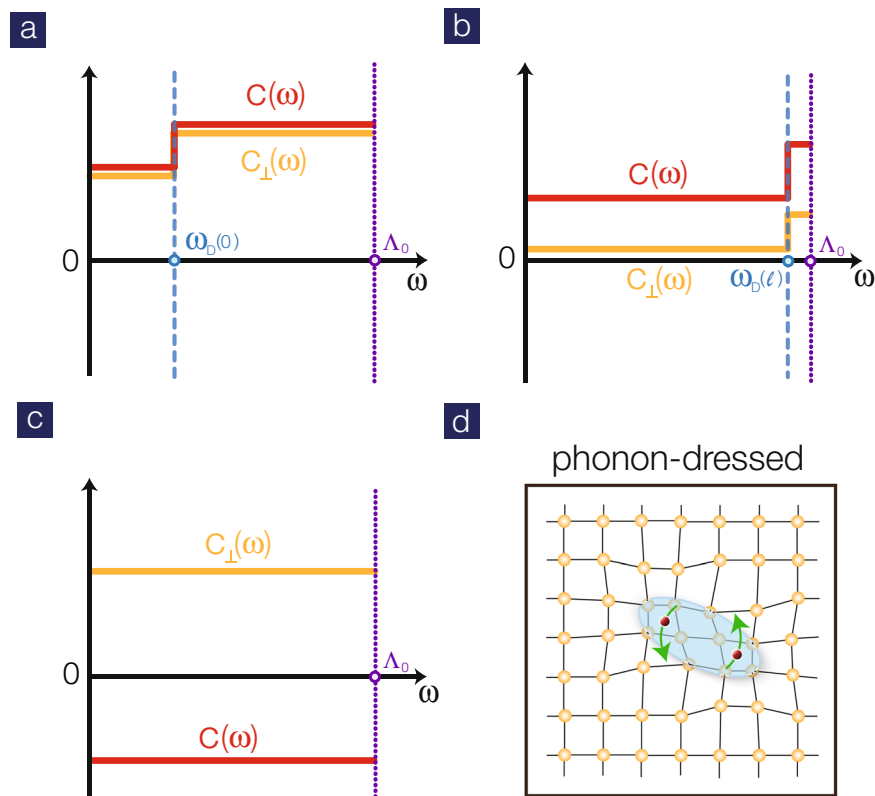
Figure 3. (**a**) Interaction profile of the dominant intra-band C and inter-band $C_\perp$ Cooper scatterings before RG transformation. (**b**) As RG progresses, the step evolves since the Debye energy is rescaled, $\omega_D(l) = \omega_D e^l$. (**c**) For $l > l_D$, the distinction between simultaneous and retarded interactions disappears. (**d**) Schematic picture for phonon-dressed unconventional superconductor.

sitive to the Debye frequency (the second term vanishes). Thus, $\alpha \approx 1/2$. On the other hand, for unconventional superconductors without relevant electron-phonon interactions, $\Delta_c \sim \Lambda_0$ and the cutoff length scale is also not sensitive to the Debye frequency. It is clear that $\alpha = 0$ in this case. But, what happens if the electron-phonon interactions, though not dominant, are actually relevant under RG transformation? We shall elaborate the details in Discussion.

Discussion

To extract the isotope exponent, we study how the cutoff length scale l_c varies with different Debye frequencies due to isotope substitutions. In weak coupling, we found that g_i are much larger than $\tilde{g}_i$. Thus, Δ_c has very weak dependence on ω_D and the first term can be ignored. The contribution from the second term is shown in Fig. 4. We tried two different profiles for the retarded interactions. Include only intra-band interactions, $\tilde{c}_{ii}(0) = -0.3\ U$ first, where U is the strength of electron-electron interactions. The isotope exponent is positive (reading from the slope), $\alpha \approx 0.1$, with very smooth variation. On the other hand, with only inter-band interactions, $\tilde{c}_{ij}(0) = -0.14\ U$, the isotope exponent is negative and changes gradually from zero to $\alpha \approx -0.03$.

These anomalous isotope effects are closely related to the unconventional pairing symmetry. For the $s_\pm$-wave pairing, $c_{ii} < 0$ but $c_{ij} > 0$ at the cutoff length scale. The phonon-mediated intra-band interactions $\tilde{c}_{ii} < 0$ help to develop the pairing instability and thus lead to a positive isotope exponent. On the other hand, the inter-band ones $\tilde{c}_{ij} < 0$ have opposite sign with their simultaneous counterparts c_{ij}. In consequence, the pairing instability is suppressed and an inverses isotope effect is in order. The RG analysis presented here provides clear and natural connection between the anomalous isotope effect and the unconventional pairing symmetry.

Although the isotope exponent α can be extracted numerically in weak coupling, extending the quantitative description to intermediate coupling may not be easy. If the pairing gaps open before hitting the Debye energy scale, i.e. $l_c < l_D$, our numerical results show that l_c solely depend on electronic interactions and thus $dl_c/dl_D = 0$. The isotope exponent in this regime mainly arises from the first term. The pairing gap $\Delta_c = \Delta_c(\Lambda_0, \omega_D e^l)$, depending on both the bandwidth and the rescaled Debye frequency, is now quite complicated. The RG analysis alone is not sufficient to obtain α in a quantitative fashion. However, we recently found that the effective Hamiltonian at the cutoff length scale is well captured by mean-field theory (not yet published). In principle, one can combine RG and mean-field approaches together to compute the isotope exponent in intermediate coupling more accurately.
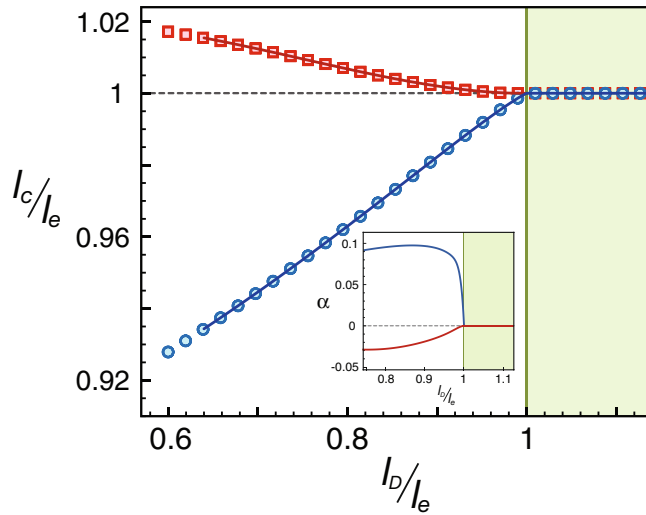
Figure 4. The cutoff length scale l_c versus l_D for inclusion of intraband interactions $\tilde{c}_{ii}(0) = -0.3\ U$ (blue circles) and interband ones $\tilde{c}_{ij}(0) = -0.14\ U$ (red square), where U is the strength of electron-electron interactions. For convenience, the axes are rescaled in the unit of l_e, the cutoff length scale with electronic interactions only. The inset shows the isotope exponent by taking numerical derivative.

In the end, we discuss the recent discovery of superconductivity in FeSe/STO systems[49,50]. We emphasize that our current approach includes fermiology, electron-electron interactions, and electron-phonon interactions within only the superconducting(SC) layers. One crucial assumption is the profile of the mediated electron-phonon inter-actions can be captured by the step function. The RG scheme built upon this approximation works as explained in the manuscript. However, according to the recent literatures in FeSe/STO systems[49–56], to include the non-SC (SrTiO$_3$) layers we need to devise a new theoretical approach which is beyond our model at this point. The profile of the electron-phonon interactions arisen from non-SC layers is probably not captured by the simple step function anymore. One needs to find out the interaction profile generated by the non-SC layers first so that one can devise the RG scheme accordingly. This is going to be an interesting and challenging topic to explore in the future.

Methods

RG equations. The interactions between these chiral fermions fall into two categories[39]: Cooper scattering c_{ij}^l, c_{ij}^s and forward scattering f_{ij}^l, f_{ij}^s. The retarded ones share the same classification, denoted with an extra tilde symbol. The RG equations for the simultaneous interactions are,

$$
\begin{aligned}
\dot{c}_{ii}^l &= -2\sum_{k\neq i}\alpha_{ii,k}c_{ik}^l c_{ki}^s - 2(c_{ii}^l)^2,\\
\dot{c}_{ii}^s &= -\sum_{k\neq i}\alpha_{ii,k}[(c_{ik}^l)^2 + (c_{ik}^s)^2] - (c_{ii}^l)^2,\\
\dot{c}_{ij}^l &= -\sum_{k}\alpha_{ij,k}[c_{ik}^l c_{kj}^s + c_{jk}^l c_{ki}^s] - 4f_{ij}^l c_{ij}^l\\
&\quad + 2f_{ij}^l c_{ij}^s + 2f_{ij}^s c_{ij}^l,\\
\dot{c}_{ij}^s &= -\sum_{k}\alpha_{ij,k}[c_{ik}^l c_{kj}^l + c_{ik}^s c_{kj}^s] + 2f_{ij}^s c_{ij}^s,\\
\dot{f}_{ij}^l &= -2(f_{ij}^l)^2 - 2(c_{ij}^l)^2 + 2c_{ij}^l c_{ij}^s,\\
\dot{f}_{ij}^s &= (c_{ij}^s)^2 - (f_{ij}^l)^2,
\end{aligned}
\tag{7}
$$

where $\dot{g} = dg/dl$, where $l = \ln(\Lambda_0/\Lambda)$ is the logarithm of the ratio between bare energy cutoff Λ_0 and the running cutoff Λ. The tensor $\alpha_{ij,k} = (v_i + v_k)(v_j + v_k)/[2v_k(v_i + v_j)]$ with v_i representing the Fermi velocities.

The second set of equations describes how the retarded interactions are renormalized,

$$
\begin{aligned}
\dot{\tilde{c}}_{ii}^l &= 2\tilde{c}_{ii}^l c_{ii}^s - 4\tilde{c}_{ii}^l c_{ii}^l - 2(\tilde{c}_{ii}^l)^2,\\
\dot{\tilde{c}}_{ij}^l &= -4\tilde{f}_{ij}^l c_{ij}^l - 4f_{ij}^l \tilde{c}_{ij}^l - 4\tilde{f}_{ij}^l \tilde{c}_{ij}^l + 2\tilde{f}_{ij}^l c_{ij}^s + 2f_{ij}^s \tilde{c}_{ij}^l,\\
\dot{\tilde{f}}_{ij}^l &= -4\tilde{f}_{ij}^l f_{ij}^l - 2(\tilde{f}_{ij}^l)^2 - 4\tilde{c}_{ij}^l c_{ij}^l - 2(\tilde{c}_{ij}^l)^2\\
&\quad + 2\tilde{f}_{ij}^l f_{ij}^s + \tilde{c}_{ij}^l c_{ij}^s.
\end{aligned}
\tag{8}
$$

Note that we separate the intra-band and inter-band couplings for clarity, i.e. $i \neq j$ in the above RG equations. In fact, the separation is necessary because we shall see later that inter-band and intra-band couplings play different roles in the low-energy limit. In addition, $f_{ii} = 0$ and $\tilde{f}_{ii} = 0$ to avoid double counting.

References

1. Kresin, V., Morawitz, H. & Wolf, S. A. *Mechanism of Conventional and High Tc Superconductivity*. (Oxford Press, Oxford, 1993).
2. Anderson, P. W. *Theory of Superconductivity in the High-Tc Cuprates*. (Princeton University Press, Princeton, 1997).
3. Paglione, J. & Greene, R. L. High-temperature superconductivity in iron-based materials. *Nature Phys.* **6**, 645–658 (2010).
4. Norman, M. R. The Challenge of Unconventional Superconductivity. *Science* **332**, 196–200 (2011).
5. Stewart, G. R. Superconductivity in iron compounds. *Rev. Mod. Phys.* **83**, 1589–1652 (2011).
6. Kresin, V. Z. & Wolf, S. A. Electron-lattice interaction and its impact on high Tc superconductivity. *Rev. Mod. Phys.* **81**, 481–501 (2009).
7. Bud'ko, S. L. *et al*. Boron Isotope Effect in Superconducting MgB_2. *Phys. Rev. Lett.* **86**, 1877–1880 (2001).
8. Iliev, M. N. *et al*. Raman phonons and ageing-related surface disorder in Na_xCoO_2. *Physica C* **402**, 239–242 (2004).
9. Lupi, S., Ortolani, M. & Calvani, P. Optical conductivity of single crystals of $Na_{0.57}CoO_2$. *Phys. Rev. B* **69**, 180506(R) (2004).
10. Uchiyama, H. *et al*. Softening of Cu-O Bond Stretching Phonons in Tetragonal $HgBa_2CuO_{4+\delta}$. *Phys. Rev. Lett.* **92**, 197005 (2004).
11. Lee, J. *et al*. Interplay of electron-lattice interactions and superconductivity in $Bi_2Sr_2CaCu_2O_{8+\delta}$. *Nature* **442**, 546–550 (2006).
12. Yokoi, M., Kobayashi, Y., Sato, M. & Sugai, S. Isotope Effect on Superconducting Transition Temperature of $Na_xCoO_2 \cdot yH_2O$. *J. Phys. Soc. Jpn.* **77**, 094713 (2008).
13. Lanzara, A. *et al*. Evidence for ubiquitous strong electron? Phonon coupling in high-temperature superconductors. *Nature* **412**, 510–514 (2001).
14. Hasan, M. Z. *et al*. Fermi Surface and Quasiparticle Dynamics of $Na_{0.7}CoO_2$ Investigated by Angle-Resolved Photoemission Spectroscopy. *Phys. Rev. Lett.* **92**, 246402 (2004).
15. Yang, H.-B. *et al*. ARPES on $Na_{0.6}CoO_2$: Fermi Surface and Unusual Band Dispersion. *Phys. Rev. Lett.* **92**, 246403 (2004).
16. Gweon, G.-H. *et al*. An unusual isotope effect in a high-transition-temperature superconductor. *Nature* **430**, 187–190 (2004).
17. Iwasawa, H. *et al*. Isotopic Fingerprint of Electron-Phonon Coupling in High-T_c Cuprates. *Phys. Rev. Lett.* **101**, 157005 (2008).
18. Giustino, F., Cohen, M. L. & Louie, S. G. Small phonon contribution to the photoemission kink in the copper oxide superconductors. *Nature* **452**, 975–978 (2008).
19. Aswathy, P. M., Anooja, J. B., Sarun, P. M. & Syamaprasad, U. An overview on iron based superconductors. *Superconductor Science and Technology* **23**, 7 (2010).
20. Chubukov, A. V. Pairing Mechanism in Fe-Based Superconductors. *Annu. Rev. Condens. Matter Phys.* **3**, 57 (2012).
21. Chen, X., Dai, P., Feng, D., Xiang, T. & Zhang, F.-C. Iron-based high transition temperature superconductors. *National Science Review* **1**, 371 (2014).
22. Chubukov, A. & Hirschfeld, P. J. Iron-based superconductors, seven years later. *Physics Today* **68**(6), 46 (2015).
23. Hosono, H. & Kuroki, K. Iron-based superconductors: Current status of materials and pairing mechanism. *Physica C* **514**, 399 (2015).
24. Boeri, L., Dolgov, O. V. & Golubov, A. A. Is $LaFeAsO_{1-x}F_x$ an Electron-Phonon Superconductor? *Phys. Rev. Lett.* **101**, 026403 (2008).
25. Granath, M., Bielecki, J., Holmlund, J. & Börjesson, L. Anharmonic softening of Raman active phonons in iron-pnictides: Estimating the Fe isotope effect due to anharmonic expansion. *Phys. Rev. B* **79**, 235103 (2009).
26. Le Tacon, M. *et al*. Inelastic x-ray scattering study of superconducting $SmFeAsO_{1-x}F_y$ single crystals: Evidence for strong momentum-dependent doping-induced renormalizations of optical phonons. *Phys. Rev. B* **80**, 220504(R) (2009).
27. Richard, P. *et al*. Angle-Resolved Photoemission Spectroscopy of the Fe-Based $Ba_{0.6}K_{0.4}Fe_2As_2$ High Temperature Superconductor: Evidence for an Orbital Selective Electron-Mode Coupling. *Phys. Rev. Lett.* **102**, 047003 (2009).
28. Liu, R. H. *et al*. A large iron isotope effect in $SmFeAsO_{1-x}F_x$ and $Ba_{1-x}K_xFe_2As_2$. *Nature* **459**, 64–67 (2009).
29. Shirage, P. M. *et al*. Inverse Iron Isotope Effect on the Transition Temperature of the $(Ba,K)Fe_2As_2$ Superconductor. *Phys. Rev. Lett.* **103**, 257003 (2009).
30. Shirage, P. M. *et al*. Absence of an Appreciable Iron Isotope Effect on the Transition Temperature of the Optimally Doped $SmFeAsO_{1-y}$ Superconductor. *Phys. Rev. Lett.* **105**, 037004 (2010).
31. Khasanov, R. *et al*. Iron isotope effect on the superconducting transition temperature and the crystal structure of $FeSe_{1-x}$. *New J. Phys.* **12**, 073024 (2010).
32. Chu, W. *et al*. Iron Isotope Effect and Local Lattice Dynamics in the (Ba, K)Fe2As2 Superconductor Studied by Temperature-Dependent EXAFS. *Scientific Reports* **3**, 1750 (2013).
33. Singh, B., Shirage, P. M., Iyo, A. & Kumar, P. Iron isotope effect in $SmFeAsO_{0.65}$ and $SmFeAsO_{0.77}H_{0.12}$ superconductors: A Raman study. *AIP Advances* **6**, 105310 (2016).
34. Khasanov, R. *Isotope Effect on the Transition Temperature Tc in Fe-Based Superconductors: The Current Status. High-Tc Copper Oxide Superconductors and Related Novel Materials* 255 (Springer, Cham, 2017).
35. Khasanov, R., Bendele, M., Bussmann-Holder, A. & Keller, H. Intrinsic and structural isotope effects in iron-based superconductors. *Phys. Rev. B* **82**, 212505 (2010).
36. Yanagisawa, T. *et al*. Isotope Effect in Multi-Band and Multi-Channel Attractive Systems and Inverse Isotope Effect in Iron-Based Superconductors. *J. Phys. Soc. Jpn.* **78**, 094718 (2009).
37. Bussmann-Holder, A. & Keller, H. Comment on "Isotope Effect in Multi-Band and Multi-Channel Attractive Systems and Inverse Isotope Effect in Iron-Based Superconductors". *J. Phys. Soc. Jpn.* **79**, 126001 (2010).
38. Zimanyi, G. T., Kivelson, S. A. & Luther, A. Superconductivity from Predominantly Repulsive Interactions in Quasi One-Dimensional Systems. *Phys. Rev. Lett.* **60**, 2089–2092 (1988).
39. Seidel, A., Lin, H.-H. & Lee, D.-H. Phonons in Hubbard ladders studied within the framework of the one-loop renormalization group. *Phys. Rev. B* **71**, 220501(R) (2005).
40. Cai, Y., Huang, W.-M. & Lin, H.-H. Renormalization-group exponents for superconducting phases in two-leg ladders. *Phys. Rev. B* **85**, 134502 (2012).
41. Okamoto, J., Mathey, L. & Huang, W.-M. Influence of electron-phonon coupling on the low-temperature phases of metallic single-wall carbon nanotubes. *Phys. Rev. B* **98**, 205122 (2018).
42. Kuroki, K. *et al*. Unconventional Pairing Originating from the Disconnected Fermi Surfaces of Superconducting $LaFeAsO_{1-x}F_x$. *Phys. Rev. Lett.* **101**, 087004 (2008).
43. Ding, H. *et al*. Observation of Fermi-surface? Dependent nodeless superconducting gaps in $Ba_{0.6}K_{0.4}Fe_2As_2$. *Europhys. Lett.* **83**, 47001 (2008).
44. Balents, L. & Fisher, M. P. A. Weak-coupling phase diagram of the two-chain Hubbard model. *Phys. Rev. B* **53**, 12133–12141 (1996).
45. Lin, H.-H., Balents, L. & Fisher, M. P. A. N-chain Hubbard model in weak coupling. *Phys. Rev. B* **56**, 6569–6593 (1997).
46. Lin, H.-H., Balents, L. & Fisher, M. P. A. Exact SO(8) symmetry in the weakly-interacting two-leg ladder. *Phys. Rev. B* **58**, 1794–1825 (1998).

47. Shih, H.-Y., Huang, W.-M., Hsu, S.-B. & Lin, H.-H. Hierarchy of relevant couplings in perturbative renormalization group transformations. *Phys. Rev. B* **81**, 121107(R) (2010).
48. Wang, F., Zhai, H., Ran, Y., Vishwanath, A. & Lee, D.-H. Functional Renormalization-Group Study of the Pairing Symmetry and Pairing Mechanism of the FeAs-Based High-Temperature Superconductor. *Phys. Rev. Lett.* **102**, 047005 (2009).
49. He, S. *et al.* Phase diagram and electronic indication of high-temperature superconductivity at 65 K in single-layer FeSe films. *Nature Materials* **12**, 605 (2013).
50. Tan, S. *et al.* Interface-induced superconductivity and strain-dependent spin density waves in FeSe/SrTiO3 thin films. *Nature Materials* **12**, 634 (2013).
51. Lee, J. J. *et al.* Interfacial mode coupling as the origin of the enhancement of T_c in FeSe films on $SrTiO_3$. *Nature* **515**, 245 (2014).
52. Fan, Q. *et al.* Plain s-wave superconductivity in single-layer FeSe on $SrTiO_3$ probed by scanning tunnelling microscopy. *Nature Physics* **11**, 946 (2015).
53. Lee, D.-H. What makes the Tc of FeSe/SrTiO3 so high? *Chin. Phys. B* **24**, 117405 (2015).
54. Tian, Y. C. *et al.* Ultrafast Dynamics Evidence of High Temperature Superconductivity in Single Unit Cell FeSe on $SrTiO_3$. *Phys. Rev. Lett.* **116**, 107001 (2016).
55. Tang, C. *et al.* Interface-enhanced electron-phonon coupling and high-temperature superconductivity in potassium-coated ultrathin FeSe films on $SrTiO_3$. *Phys. Rev. B* **93**, 020507(R) (2016).
56. Wang, Q.-Y. *et al.* Interface-Induced High-Temperature Superconductivity in Single Unit-Cell FeSe Films on SrTiO3, *Chin. Phys. Lett.* **29**, 037402 (2012).

Acknowledgements

Author Contributions

Both W.M.H. and H.H.L. contribute extensively to the work in all aspects. W.M.H. and H.H.L. prepare the manuscript together.

Additional Information

Competing Interests: The authors declare no competing interests.

Publisher's note: Springer Nature remains neutral with regard to jurisdictional claims in published maps and institutional affiliations.